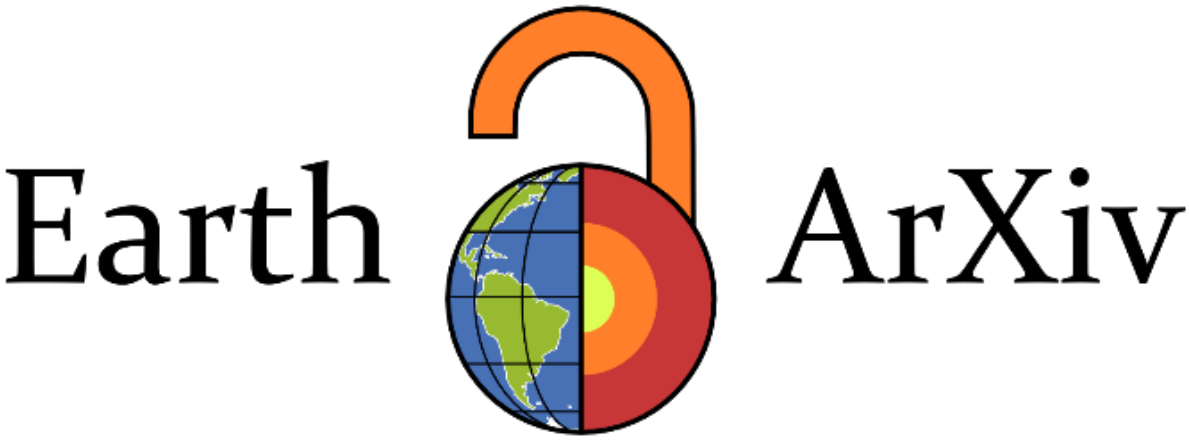

Accounting for uncertainty from internal variability in global-temperature based attribution of climate extremes with single realisations

Maximilian Kotz,[a, b, c] Markus Donat,[a, d]

[a] *Barcelona Supercomputing Center, Barcelona, Spain*

[b] *Potsdam Institute for Climate Impact Research, Potsdam, Germany*

[c] *Centre for Biodiversity and Conservation Science, University of Queensland, Brisbane, Australia*

[d] *Institució Catalana de Recerca i Estudis Avançats (ICREA), Barcelona, Spain*

Corresponding author: Maximilian Kotz, maximilian.kotz@bsc.es

ABSTRACT

Attribution of regional climate change to anthropogenic forcing within the single realisation available from observations is an important but challenging goal for statistical methods in climate science. Correlating regional conditions with global temperatures is a popular approach, especially for attributing downstream impacts on human health or the economy. However, the influence of internal variability on such approaches remains unquantified. Here, we use large ensembles from three climate models to quantify the role of internal variability for attribution of climate extremes. For temperature extremes, internal variability brings uncertainties exceeding 40% of the climate change signal across 50, 38, and 9% of the global surface area in the MIROC6, MPI-ESM1-2-LR and CanESM5 models respectively. We furthermore show that these uncertainties can be accurately inferred from individual ensemble members using a block-bootstrap procedure - offering potential for application to observations. For precipitation extremes however, relative uncertainties are substantially larger, exceeding 100% across 90%, 75% and 55% of the global surface area in the three models used, and the block-bootstrapping fails to replicate the uncertainty of the large ensemble - although spatial aggregation reduces the discrepancies between them to some extent. This work provides a basis for the attribution of temperature extremes from observations which can robustly capture the uncertainty driven by internal climate variability, but indicates the need for caution when applying such approaches to noisier variables such as precipitation.

SIGNIFICANCE STATEMENT

Attributing climate change to human forcing is crucial to many aspects of climate policy regarding adaptation, mitigation and climate justice. Approaches which correlate local climate with global temperature using observations alone are particularly popular for the attribution of climate impacts on the economy and human health. Confidence in these methods relies on the correlations having been unlikely to occur due to internal variability alone. We test these approaches with large ensembles, finding large uncertainties due to internal variability sufficient to preclude robust attribution in certain regions. We also show that for temperature extremes, these uncertainties can be recovered from individual ensemble members via block-bootstrapping. This provides a robust basis for attribution of temperature extremes and their impacts with observations alone.

1. Introduction

As global temperatures continue to rise and pass internationally agreed limits (Copernicus 2025), understanding the impacts of climate change gains further relevance. The increasing exposure to high temperature and heavy precipitation extremes is of particular concern given their known impact on socioeconomic (Kotz et al. 2022; Callahan and Mankin 2022a; Davenport et al. 2021; Dasgupta et al. 2021) and natural systems (Kotz et al. 2025; Murali et al. 2023). At the regional level, these extremes increase in intensity quasi-linearly with global mean surface temperature and therefore with increasing cumulative human emissions (Seneviratne et al. 2016). Formalising the attribution of these extremes and their impacts to human influence remains an important and active area of climate science with ongoing challenges and developments (Trok et al. 2024; Clarke et al. 2022), especially for attribution of impacts (King et al. 2023; Noy et al. 2023).

Numerical simulations from General Circulation and Earth System Models (GCMs/ESMs) under different historical forcing scenarios have played a crucial role in the attribution of climatic changes and their impacts (Ortiz-Bobea et al. 2021; Diffenbaugh and Burke 2019) - especially within the framework of the Detection and Attribution Model Intercomparison Project (Gillett et al. 2016) where simulations are run under counterfactual historical scenarios with different anthropogenic emissions removed. The development of large ensembles of climate models under different initialisations have also been valuable in separating human-forced changes from internal variability (Deser et al. 2020). As a complementary approach, statistical methods offer possibilities to detect externally driven climatic changes from a single realisation of the climate system directly within observations (Wills et al. 2020, 2025). These approaches offer value due to their lower computational requirements and the avoidance of certain biases which climate models are known to exhibit (Wills et al. 2022; Donat et al. 2023).

Amongst these statistical methods, the correlation of regional climate conditions with global temperatures has become a popular choice, especially for the attribution of downstream climate impacts to human influence (Mengel et al. 2021). These methods are motivated by the fact that virtually all of the observed historical global warming signal (0.84-1.10C

between 1850-1900 and 2001-2020) is attributable to human influence (likely range of human contribution of 0.8-1.3C) (Lee et al. 2023) and that forced changes in extremes - amongst other characteristics - are known to scale with global temperatures (Seneviratne et al. 2016). A further advantage is the ability to evaluate the changes in conditions associated with particular levels of global warming, allowing their further connection and attribution to individual sources of emissions (Quilcaille et al. 2025; Callahan and Mankin 2025, 2022b). The application of such attribution approaches to quantifying downstream impacts has grown rapidly across diverse fields from agriculture (Ortiz-Bobea et al. 2021) and the economy (Diffenbaugh and Burke 2019) to human health (Carlson et al. 2025; Beck et al. 2024) and biodiversity (Kotz et al. 2025), and has potential to inform policy making and even legal proceedings in relation to loss and damage (Tavoni et al. 2024).

Despite the promise of these methods, the role of internal climate variability in confounding global-temperature based attribution approaches remains largely unquantified. For example, widely-used sources of counterfactual climate data for impact attribution based on this approach do not yet provide quantification of uncertainty at all (Mengel et al. 2021; Dimitrova et al. 2024). Even in studies which do provide estimates of uncertainty, the extent to which this reflects the role of internal climate variability remains unclear (Beck et al. 2024). Given the substantial contributions of internal variability to regional climate trends (Hawkins and Sutton 2009; Lehner et al. 2020), especially under historical levels of anthropogenic forcing and for variables such as precipitation (Deser et al. 2012), this represents a major limitation in the development of robust impact-attribution statements.

Our paper aims to quantify the role of internal variability in these attribution methods, using large ensembles of climate models as an idealised setting to test these approaches. Large ensembles involve simulations of a given climate model under the same climate forcing, with variations in initial conditions used to generate diverse realisations of internal climate variability within which the ensemble mean represents the expected response to forcing. Our paper has three main objectives: (1) to quantify the uncertainty in the relationships between global temperature and regional climate conditions driven by internal variability; (2) to test whether statistical methods like bootstrapping could theoretically infer these uncertainties when applied to individual realisations of the climate system; and (3) to apply such methods

to observational data. We focus our analysis on the frequency and intensity of climate extremes, given their important role for impacts as reflected in recent work on the economy (Callahan and Mankin 2025) and biodiversity (Kotz et al. 2025). We furthermore consider both temperature and precipitation extremes, to explore variables for which the relative importance of internal variability and anthropogenic forcing differs.

2. Methods

Data

We use data of daily surface temperature ("tas") and precipitation ("pr") from three Earth System Models providing large ensembles within the Coupled Model Intercomparison Project phase 6 (Eyring et al. 2016) (CanESM5, MIROC6 and MPI-ESM1-2-LR), each with 50 ensemble members based on different initialisations. We primarily use data from simulations under the historical forcing scenario, using data from 1940 onwards to replicate the time-frame of availability in major observational data products like the ERA-5 reanalysis (Hersbach et al. 2020). We additionally use data from simulations for the period 2015-2024 under the SSP5-8.5 forcing scenario, to provide a full time-series until 2024 which more closely matches the ERA-5 timeseries. We use SSP5-8.5 which has closely followed historical cumulative emissions within this timeframe (Schwalm et al. 2020), but note that the radiative forcing is similar across other scenarios between 2014 and 2024 (Riahi et al. 2017) and would therefore likely provide similar results. Moreover, we emphasise that we only use these simulations to test attribution methodologies in an idealised setting rather than to make predictions about developments over the period 2015-2024. We also use data on daily surface temperature and precipitation from the ERA-5 reanalysis for the period 1940-2024 (Hersbach et al. 2020).

Climate extreme metrics

We use two complementary metrics to capture the intensity and frequency of climate extremes. We use the annual maximum of 5 day averages of daily temperature and precipitation ($TX5d$, $PX5$d) to measure the intensity of multi-day climate extremes which are relevant for impacts (Callahan and Mankin 2025). We also use the annual number of days exceeding the 99th percentile of the historical distribution ($T99p, P99p$) - using the period 1940-1970 and a consideration of all seasons to define these thresholds. This choice focuses

on the exceedance of absolute temperature and precipitation thresholds rather than seasonally-defined thresholds, as has been shown to be relevant for impacts (Kotz et al. 2025). We use the threshold obtained from the historical period of each ensemble member separately (rather than taking an average across ensemble members), such that each ensemble member is treated independently as would be the case when applying such attribution methods to observations which we aim to test.

Global-temperature based attribution

The climate impact attribution literature typically uses smoothed global mean temperatures to learn a relationship between large-scale forcing and local climate conditions, with which to then detrend local climate conditions and generate a counterfactual (Mengel et al. 2021). We calculate global mean surface temperature as the area weighted surface temperature ($GMT_{m,y}$) for each ensemble member (m), and smooth it with an 11-year running mean centred on the year of interest. We then fit relationships between smoothed global mean surface temperatures ($GMT_{m,y}$) and local climatic conditions ($TX5d_{m,x,y}$, $PX5d_{m,x,y}$, $T99p_{m,x,y}$, $P99p_{m,x,y}$) for each ensemble member, m, using either linear OLS models for the climate extreme intensity metrics:

$$TX5d_{m,x,y} = \beta_{m,x}\,\widetilde{GMT}_{m,y} + \alpha_{m,x} + \epsilon_{m,x,y} \quad (1)$$

or a Poisson model for the climate extreme frequency metrics:

$$log(E(T99p_{m,x,y} \mid \widetilde{GMT}_{m,y})) = \beta_{m,x}\,\widetilde{GMT}_{m,y} + \alpha_{m,x} + \epsilon_{m,x,y}\ , \quad (2)$$

where $\beta_{m,x}$ is the linear relationship between global temperatures and local climate extremes for each ensemble member and grid cell, x, $\alpha_{m,x}$ is the intercept, and $\epsilon_{m,x,y}$ the error term. We note that the local climate conditions themselves are not smoothed. The attributable climate change signal essentially depends on the estimates of $\beta_{m,x}$, which represents the scaling relationship between global mean temperature and local extremes, and on which we therefore focus our assessment of uncertainty due to internal climate variability.

Uncertainty due to internal variability

We evaluate uncertainty in climate impact attribution approaches due to internal variability based on the spread of estimates of $\beta_{m,x}$ across ensemble members. We express this through

the relative error, measured as the ratio of the standard deviation, , to the mean, , of these estimates across ensemble members:

$$\chi_x = 100 * \frac{\sigma_x(\beta_{m,x})}{\mu_x(\beta_{m,x})}. \quad (3)$$

We proceed with these calculations separately for each climate extreme metric and each of the three large ensembles.

Block-bootstrap estimates of uncertainty

The multiple realisations of the simulated climate system within the large ensembles provide an idealised setting in which to evaluate the uncertainty due to internal variability inherent in these climate impact-attribution approaches. However, approaches based on observations will always be constrained to work with a single realisation of the climate system. We therefore propose block-bootstrapping as a potential method to infer estimates of uncertainty from individual realisations which might reflect the uncertainty driven by internal variability. Similar approaches have been used to construct so-called "observational large ensembles" (McKinnon and Deser 2018; McKinnon et al. 2017) and we draw on the intuition of these approaches in the context of attribution.

A crucial part of the block-bootstrapping approach is the choice of block width, which should balance the competing objectives of (i) capturing time-frames of sufficient length to represent key processes contributing to uncertainty, and (ii) to remain short enough to enable a sufficiently large number of potential bootstrap samples. To choose the block width, we calculate the autocorrelation function of the residuals from the regressions between global temperatures and local climate conditions, using the actual residuals in the case of the extreme intensity metrics and the residuals on the deviance scale for the Poisson regressions applied to the frequency metrics - both of these are represented as $\epsilon_{m,x,y}$ in equations (1) and (2). We use plots of the autocorrelation strength to guide the choice of block widths, and explore results under a range of block widths as outlined in the results section. Variance estimates of the autocorrelation functions are calculated using Bartlett's formula (Bartlett 1946) and two sided significance tests are calculated for each ensemble member.

The autocorrelation functions are then used to determine the block width for the block-bootstrap of the joint time series of local climate extremes and global temperatures. We apply consistent block sampling across different grid-cells and different members of the same large ensemble, and then re-evaluate the regressions outlined in equations (1) and (2). We use 100 samples with replacement ($N_s = 100$). These provide us with a distribution of the relationship between global temperature and local climate extremes for each individual ensemble member, $\hat{\beta}_{s,m,x}$, with which we can estimate the relative uncertainty in these relationships derived from the bootstrap:

$$\hat{\chi}_{m,x} = 100 * \frac{\sigma_{m,x}(\beta_{s,m,x})}{\mu_{m,x}(\beta_{s,m,x})}. \quad (4)$$

Note that this estimate of relative uncertainty via bootstrapping is therefore available for each individual ensemble member. We then compare estimates of uncertainty derived from the bootstrap approach (equation 4) to those derived from the true ensemble (equation 3), to test the ability of the bootstrap to reproduce uncertainty due to internal variability as estimated from the large ensemble simulations. We do so based on a weighted pattern correlation statistic, and estimates of the fraction of the global surface area with a certain level of relative uncertainty (see Results).

The relative uncertainty is poorly defined in regions where $\mu_{m,x}$ approaches zero, and in some instances can therefore diverge strongly and bias the values of the weighted pattern correlation statistics. For the calculation of the weighted pattern correlation statistics, we therefore cap values of relative uncertainty at 100%. This choice is also motivated by the fact that values of relative uncertainty greater than 100% reflect instances of signal-to-noise ratio less than 1 in which a robust attribution to human influence is essentially not possible. Differences in values already greater than 100% are therefore not of substantial interest in the context of attribution. Increasing this cap to higher values typically reduces the values of the pattern correlations - for example, increasing the cap to 200% roughly decreases the values shown in Figure 3 by 0.1.

Finally, we apply the block-bootstrap procedure outlined here to the historical observations of ERA-5, carrying out the procedures described above with the distinction that in this case only one realisation of the climate system is available. We note that in the context of observations where only a single realisation is available, no assessment of the forced-response in terms of

the mean across realisations of internal variability can be made, but an assessment of uncertainty in the observed response due to internal variability is possible (McKinnon et al. 2017).

3. Results

Internal variability generates diverse attribution outcomes for temperature extremes

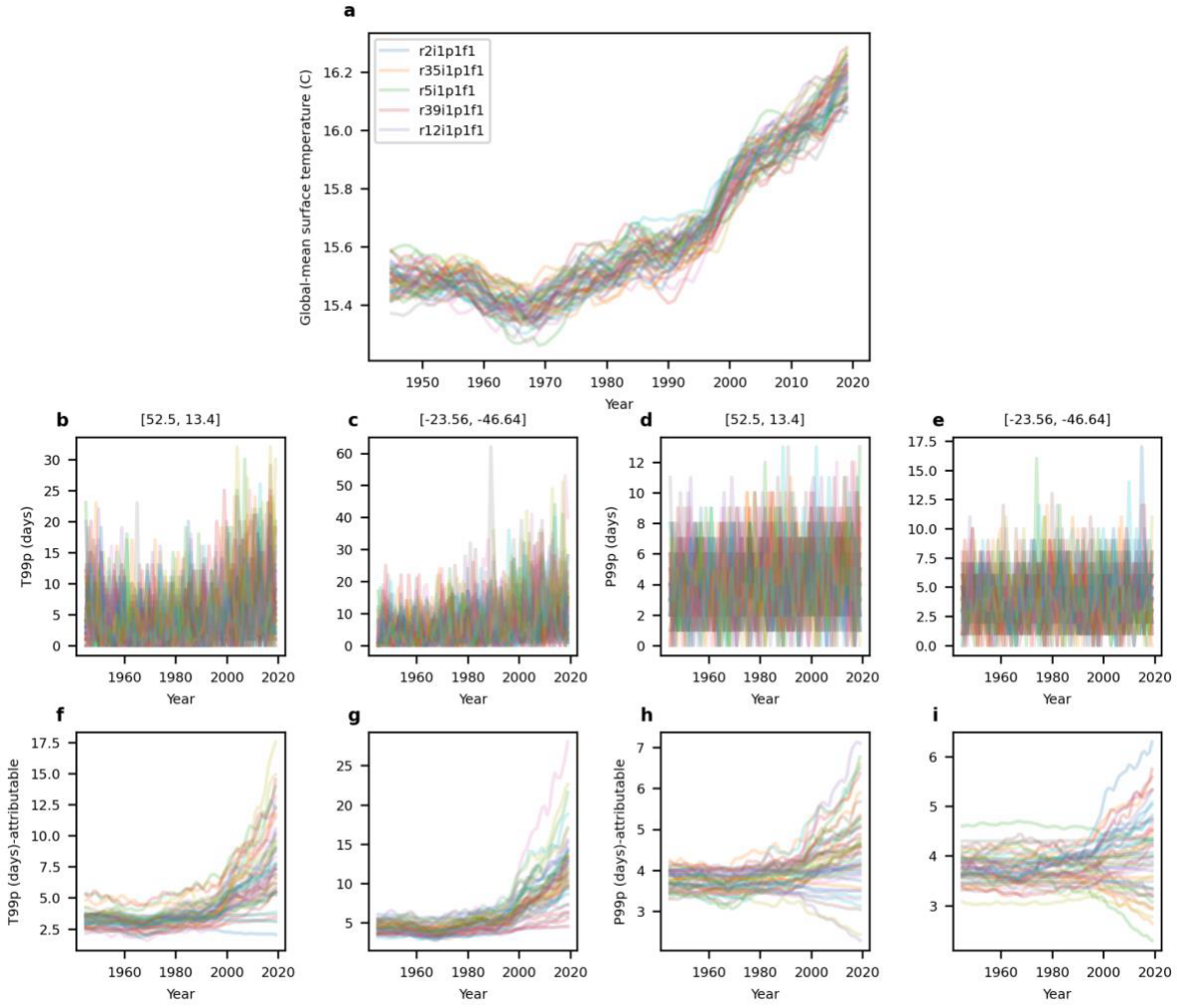

Figure 1. Internal variability generates diverse relationships between global temperatures and local climate extremes. (a) Global temperatures smoothed with an 11-year centred running mean from 50 members of the MIROC6 ensemble under historical (1945-2014) and SSP585 (2015-2020) forcing. The names of only five are highlighted in the figure legend. The annual number of days exceeding the 99th percentile of temperature (b, c) and precipitation (d, e) across the members of the MIROC6 ensemble under the same forcing, for grid-cells in Berlin and Sao Paolo (the coordinates in degrees latitude and longitude are indicated above each panel). The variation of local temperature (f, g) and precipitation extremes (h, i) which is considered "attributable" based on the regression with global mean temperature (based on a Poisson regression, see Methods).

Comparing global temperatures and regional climate extremes across realisations of the same climate model under the same forcing, we see that local climate extremes can evolve in diverse

246 ways despite similar evolutions of the global mean temperature (Figure 1a-e). Moreover, the
247 component of local climate extremes which is correlated with global mean temperatures also
248 differs substantially across different realisations of the same model (Figure 1f-i). This
249 highlights the diverse outcomes which could be attributed to human-induced climate change
250 under observationally-derived attribution approaches due to the uncertainty generated by
251 internal variability. Figure 1 shows examples for the frequency of temperature and precipitation
252 extremes ($T99p$, $P99p$), while Supplementary Figure 1 shows similar behaviour for the
253 intensity of extremes ($TX5d, PX5d$).
254
255 To formally quantify the role of internal variability, we calculate the relative uncertainty
256 (standard deviation as a percentage of the mean) in the coefficients of the regressions between
257 global mean temperature and local climate extremes across different realisations of the same
258 climate model. For temperature extremes, we see diversity across regions and climate models
259 in the magnitude of uncertainty due to internal climate variability (Figure 2a, e, i). Uncertainty
260 is largest in the Southern Ocean and South-East Pacific, where it exceeds 100% in many regions
261 in all models. Such high levels of uncertainty are also found across further widespread areas in
262 the MIROC6 and MPI-ESM1-2-LR climate models, particularly across central Africa, the
263 Indian sub-continent and Tibetan plateau. In general, CanESM exhibits generally lower levels
264 of uncertainty implying a less substantial role of internal variability for temperature extreme
265 changes.
266
267 We note that levels of uncertainty above 100% imply a signal to noise ratio between the forced
268 climate change signal and internal variability of less than 1, which would typically preclude a
269 robust statement regarding attribution of human-driven temperature extreme change. This
270 demonstrates the importance of accounting for uncertainty due to internal climate variability
271 in observationally-derived attribution approaches. Nevertheless, for temperature extremes
272 80%, 85% and 95% of the global area exhibits uncertainties less than 100% for MIROC6, MPI-
273 ESM1-2-LR and CanESM5 respectively, and 50, 62, and 91% exhibit uncertainties under 40%
274 (Figure 3a). Our analysis of these models therefore suggests that robust attribution with single
275 realisations for temperature extremes may be feasible across large areas of the Earth. However,
276 the diverse levels of uncertainty between climate models begs the question of what the true
277 level of uncertainty in observations may be, and whether this could be inferred directly from
278 observations.

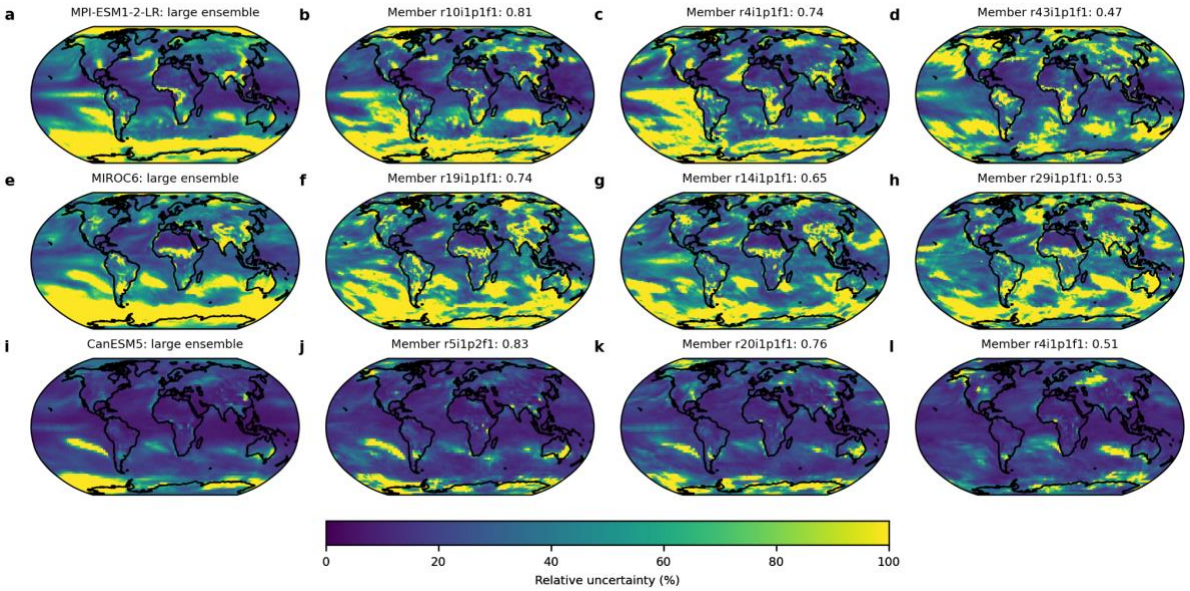

Figure 2. Uncertainty in the attribution of heat extreme frequency due to internal variability in the large ensembles and as inferred from block-bootstrapping of individual ensemble members. The relative uncertainty (ratio of standard deviation to the mean) of the correlation between global temperatures and the frequency of temperature extremes, estimated from the large ensemble (a, e, i) and by block-bootstrapping individual ensemble members (b-d, f-h, j-l). Examples are shown for three ensemble members with the highest (b, f, j), median (c, g, k) and lowest (d, h l) weighted pattern correlation between their uncertainty and that derived from the large ensemble. These weighted pattern correlations are shown above the map for each ensemble member. Results are shown for the MPI-ESM1-2-LR (a-d), MIROC6 (e-h) and CanESM5 (i-l) models.

Reproducing uncertainty from individual realisations with a block-bootstrap

We suggest that block-bootstrapping may offer the potential to infer the uncertainty due to internal climate variability from single realisations, which would imply potential for a robust application to observations. This hypothesis is partially motivated by "observational large ensembles" which have successfully used bootstrapping to develop ensembles of temperature trends from observations which accurately reflect the uncertainty due to internal variability (McKinnon et al. 2017). Block-bootstrapping individual ensemble members and re-calculating the relative uncertainty across bootstrap samples produces patterns of uncertainty which match those derived from the large ensemble well for temperature extremes (Figure 2b-d, f-h, j-l). We especially note that bootstrapping appears able to accurately capture the differences between climate models (comparing different rows of Figure 2). In general, block-bootstrapping skilfully reproduces the fractions of the global land-area under different levels of uncertainty (Figure 3a). Furthermore, weighted pattern correlations between the uncertainty maps derived from the large ensemble and the block-bootstrapped ensemble members are generally high,

with a median value of 0.65, 0.74 and 0.76 for MIROC6, MPI-ESM1-2-LR and CanESM5 respectively (Figure 3b).

These results are derived with a block width of 5 years, based on a conservative choice to capture all significant autocorrelation seen in the residuals between global temperatures and temperature extremes (Figures S2-4). We note that shorter block widths perform almost equivalently well in terms of reproducing the uncertainty from the large ensemble, with only minor under-estimation of uncertainty when using a block width of only 1 year (i.e. a normal bootstrap) (Figure A5). Using larger block widths - such as 10 years (Figure A6) - substantially reduces the ability of the bootstrap to reproduce both the patterns and magnitude of uncertainty seen in the large ensemble. The results so far described pertain to the frequency of exposure to temperature extremes ($T99p$). We note that very similar results are obtained for the intensity of temperature extremes ($TX5d$), as presented in Figures S7 and S8.

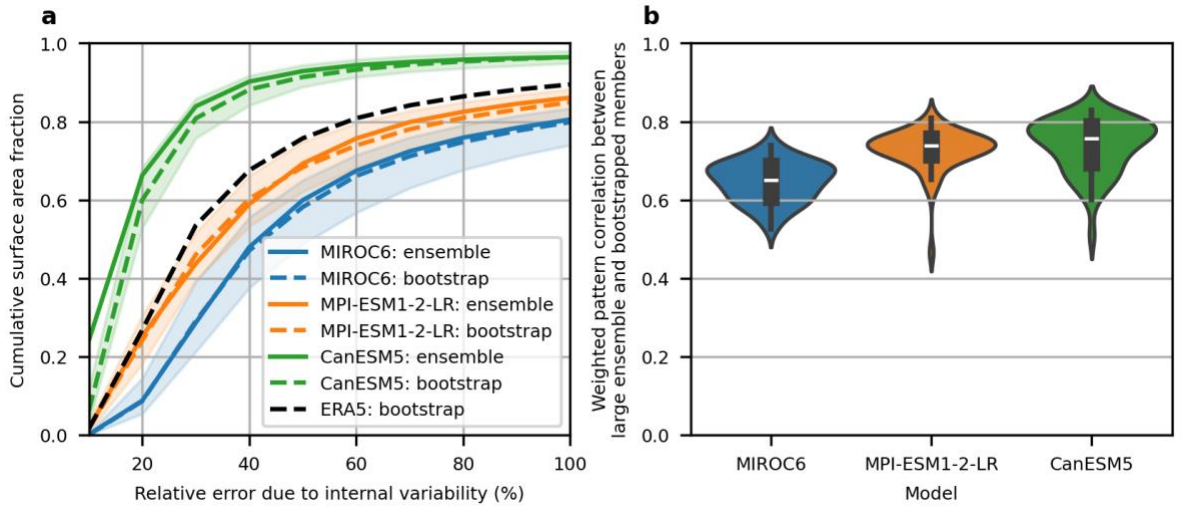

Figure 3. Comparing uncertainty in temperature extreme frequency attribution between the large ensemble and the block-bootstrapping of individual ensemble members. (a) The cumulative surface area fraction under different levels of relative uncertainty estimated from the true ensemble (solid line) and block-bootstrapped individual ensemble members (median across ensemble members: dashed line, 5-95th percentile range across ensemble members: shaded). Results of applying the same block-bootstrap procedure to the ERA5 historical reanalysis are shown in the black dashed line. (b) The distribution of weighted pattern correlations between relative uncertainty estimates from the large ensemble and the bootstrapped ensemble members. Relative uncertainty is for the correlations between global temperatures and the frequency of temperature extremes as displayed in Figures 1 and 2.

Uncertainty in attribution of precipitation extremes

Turning our attention to precipitation extremes, we note that for the examples selected in Figure 1, local precipitation extremes can show even more diverse relationships with global temperatures due to different realisations of internal variability. When quantifying this

contribution globally, we see much larger uncertainty compared to temperature (Figure 4, noting the colour scale now extending to 200% rather than 100% as in Figure 2). Relative uncertainty within the large ensemble exceeds 100% for approximately 90%, 75% and 55% of the global surface area in the MIROC6, MPI-ESM1-2-LR and CanESM5 models respectively (Figure 5a). We note that these substantially higher levels of uncertainty compared to temperature extremes are to be expected given the much stronger role of internal variability compared to human forcing for precipitation (Deser et al. 2012). The patterns of uncertainty are also distinct across climate models, although lower uncertainty is observed across central Africa and Northern mid-to-high latitudes in all three models.

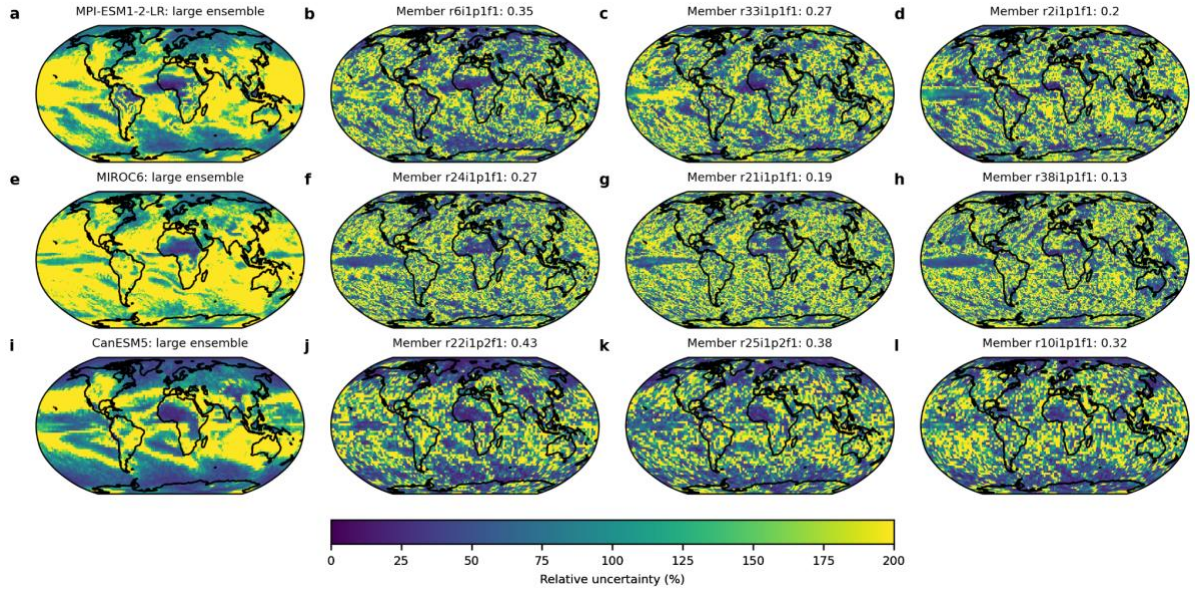

Figure 4. Relative uncertainty in attribution of precipitation extreme frequency due to internal variability in the large ensembles and block-bootstrapping of individual ensemble members. The relative uncertainty of the correlation between global temperatures and the frequency of precipitation extremes estimated from the large ensemble (left column). The relative uncertainty estimated by block-bootstrapping individual ensemble members (right columns), for the member with the best, median and worst pattern correlation compared to the uncertainty derived from the large ensemble (respectively left to right). Results are shown for the MPI-ESM1-2-LR (top row), MIROC6 (second row) and CanESM5 (lower row) models.

Investigating the capacity of the block-bootstrap approach to capture these uncertainties within individual ensemble members, we see that it performs considerably worse than in the context of temperature extremes (Figure 4). Extensive small-scale spatial variability in the relative error is present in the bootstrapped estimates of uncertainty which does not reflect the uncertainty measured in the large ensemble. Pattern correlations between the uncertainty derived from the large ensemble and the block-bootstraps are also much lower (Figure 5b), and the block-bootstrap typically underestimates uncertainty by a substantial margin (Figure 5a). Further

analysis indicates that this discrepancy is primarily driven by the average correlations between global temperatures and precipitation extremes. These correlations exhibit large discrepancies between the large ensemble average and individual ensemble members, particularly at small spatial scales (Figure A9). By contrast, the standard deviation of correlations identified with the block-bootstrap approach shows close agreement with that identified by the large ensemble (Figure A9). Equivalent analysis for the intensity of precipitation extremes ($PX5d$) shows very similar results in terms of larger uncertainty and poor reproduction by the block-bootstrap (Figure A10, 11).

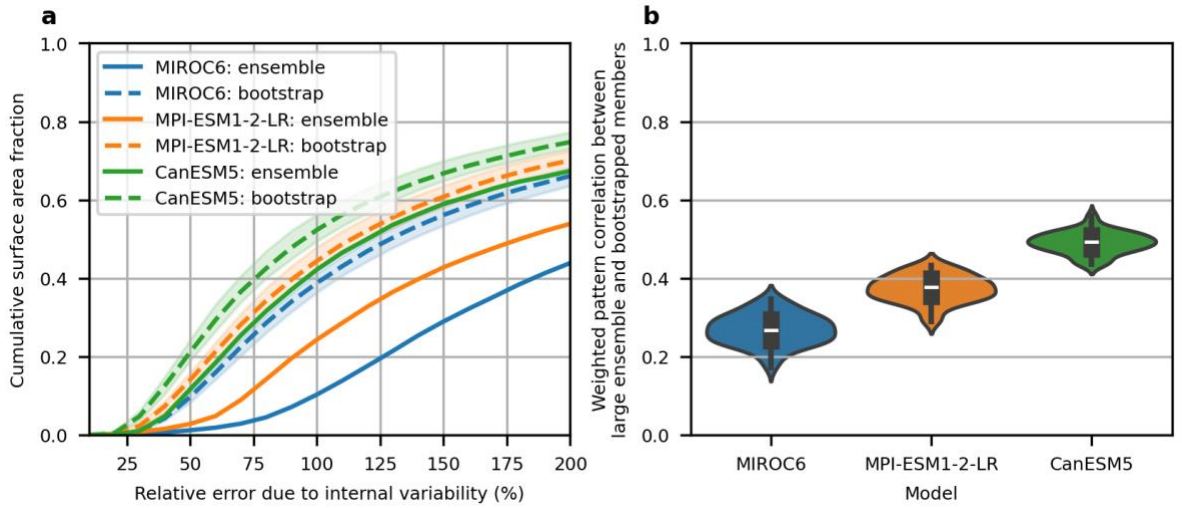

Figure 5. Comparing uncertainty in precipitation extreme frequency attribution between the large ensemble and the block-bootstrapping of individual ensemble members. (a) The cumulative surface area fraction under different levels of relative uncertainty estimated from the true ensemble (solid line) and bootstrapped ensemble members (median across ensemble members: dashed line, 5-95th percentile range: shaded). Note the extended x-axis scale compared to Figure 3. (b) The distribution of weighted pattern correlations between relative uncertainty estimated from the true ensemble and the bootstrapped ensemble members.Relative uncertainty is for the correlations between global temperatures and the frequency of precipitation extremes as displayed in Figure 4.

Spatial aggregation improves representation of internal variability for precipitation extremes

Given that small-scale features appear to drive the poor performance of the block-bootstrap for precipitation extremes, we explore whether spatial aggregation could improve its performance. This follows work indicating that spatially aggregated climate extremes exhibit changes which are much more robust to internal variability (Fischer et al. 2013). Aggregating precipitation extremes spatially to scales of five to ten degrees before running the attribution procedures notably reduces the levels of uncertainty due to internal variability and also improves the ability

of the block-bootstrap to capture this uncertainty (Figure A12). However, discrepancies in the spatial pattern of uncertainty between the large ensemble and the block-bootstrapped individual members are still substantially larger than in the case of temperature extremes even under this spatial aggregation. This suggests that averaging over larger spatial scales removes some of the internal variability which contributes to limitations in the attribution approaches, but substantial sources of internal variability across larger spatial scales remain which are not well captured by the block-bootstrap. This likely reflects the important role of large scale modes of climate variability like the Pacific Decadal Oscillation or North Atlantic Oscillation for precipitation, which exert influences over larger spatial domains and longer-timescales, making the application of a bootstrapping approach to capture this variability challenging within an observational time-series of relatively short length.

4 Discussion

To confidently attribute impacts to climate change one must be clear that they would have been unlikely to occur due to internal climate variability alone. Our work provides a formalised framework in which to assess whether approaches for attribution from a single realisation using correlations with global temperatures currently meet this criteria (Kotz et al. 2025; Mengel et al. 2021; Park et al. 2024; Dimitrova et al. 2024; Beyer et al. 2024), and whether improvements may enable them to do so.

Our first contribution is to show that internal variability contributes substantial uncertainties to these attribution approaches, generating relative uncertainties exceeding 100% across large parts of Earth, even for temperature extremes. For precipitation extremes, the contribution of internal variability is much larger, and both examples make the case that internal variability should be considered in these approaches to ensure robust uncertainty estimates for climate attribution statements. Current approaches which do not capture this source of uncertainty (Mengel et al. 2021) likely over-state the confidence of attribution to human influence, particularly for heavy precipitation extremes.

However, our second contribution is to show that robust uncertainty estimates can be derived for observationally-based attribution statements for temperature extremes. The block-bootstrap approach is easy to implement and offers an estimate of uncertainty which closely matches that which a large ensemble would provide (Figure 3). This means researchers may work with

observations rather than climate models to benefit from lower computational costs and better representation of the forced climate system and still attain attribution statements which accurately capture the role of internal variability for temperature extremes. However, our work indicates that observationally-derived attribution statements with robust uncertainty estimates are likely not possible for precipitation extremes at current levels of global warming, at least at local scales. Aggregation to larger spatial scales appears to reduce uncertainties and improve the performance of the bootstrap, but discrepancies in the spatial patterns of uncertainty still persist between the large ensemble and the bootstrap estimates even at aggregation to scales of five and ten degrees. Future work could consider incorporating indices of large scale climate variability in order to better capture sources of inter-annual to multi-decadal internal variability which may not be well captured by the current block-bootstrap approach.

An important limitation of our work is that we considered only high temperature and heavy precipitation extremes. While this choice was necessary to contain the scope of our analysis and to focus on impact-relevant variables, other climate variables may exhibit different behaviour. The strong consistency between the frequency and intensity of temperature extremes (Figure 2 and Figure A7) indicates that some generalities may exist across the temperature distribution, but further analysis will be beneficial for exploring other variables more thoroughly.

Our study has focussed on the application of this approach to observationally-derived attribution statements (Mengel et al. 2021), but we note that the results are relevant to a number of other methods. Two important contexts are pattern scaling approaches (Tebaldi and Arblaster 2014) and climate model emulators (Byers et al. 2025; Quilcaille et al. 2025), both of which derive relationships between local climate conditions and global mean temperature from multi-model ensembles like CMIP6. Our work indicates that observations could be used directly to identify these relationships, substantially reducing computational demands without limiting the representation of uncertainty due to internal variability. Most importantly, our work provides a formal basis from which to use observations alone to attribute changes in temperature extremes and their impacts to human influence while robustly capturing the uncertainty driven by internal climate variability.

Data Availability Statement.

Temperature and precipitation data from ERA5 are publicly available from Copernicus (https://cds.climate.copernicus.eu/datasets/reanalysis-era5-single-levels?tab=overview). Temperature and precipitation data from the three CMIP6 models used are available publicly from the Earth System Grid Federation (https://esgf.github.io/). Specific data and code for this analysis will be made available upon request.

Acknowledgements

The authors have no competing interests to declare. MK gratefully acknowledges the support of the European Union's Horizon 2020 research and innovation programme under the Marie Skłodowska-Curie grant agreement no. 101148359.

APPENDIX

Additional figures

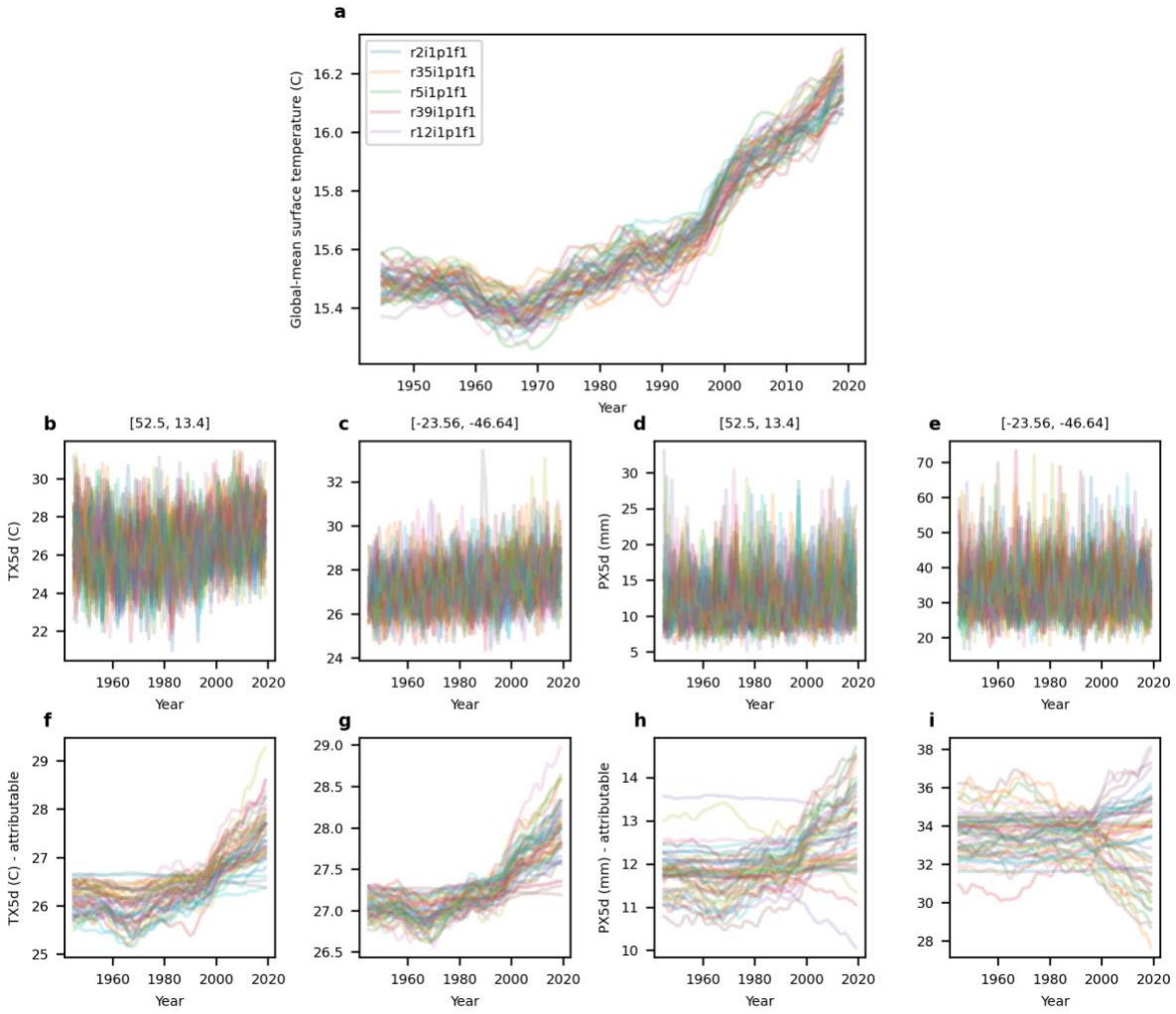

Figure A1. Internal variability generates diverse relationships between global temperature and local climate extreme intensity. The structure of the Figure is the same as Figure 1, but results are shown for the intensity of climate extremes, based on the annual maximum of 5 day average of daily surface temperature and precipitation ("TX5d" and "PX5d").

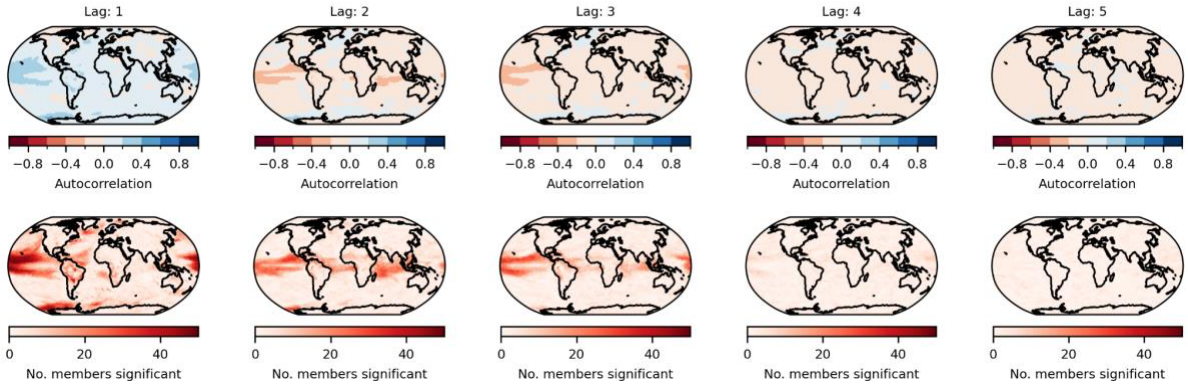

Fig. A2. Autocorrelation of the residuals of the global temperature to local extremes regression. The upper row shows the autocorrelation values, averaged across ensemble members of MPI-ESM1-2-LR. The lower row shows the number of ensemble members with autocorrelation values which are significant at the 5% level based on a two-sided significance test. Uncertainty in the autocorrelation values are calculated based on the Bartlett formula.

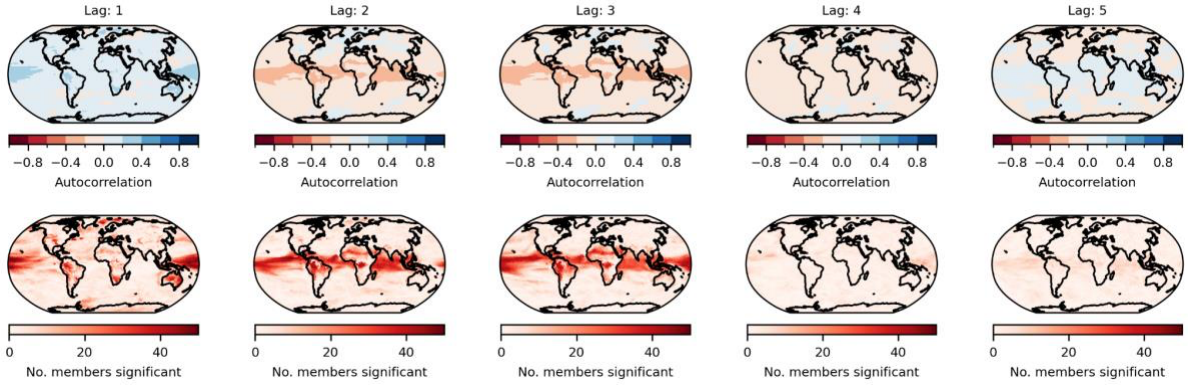

Fig. A3. Autocorrelation of the residuals of the global temperature to local extremes regression for the MIROC6 model. Details as in Fig. A2.

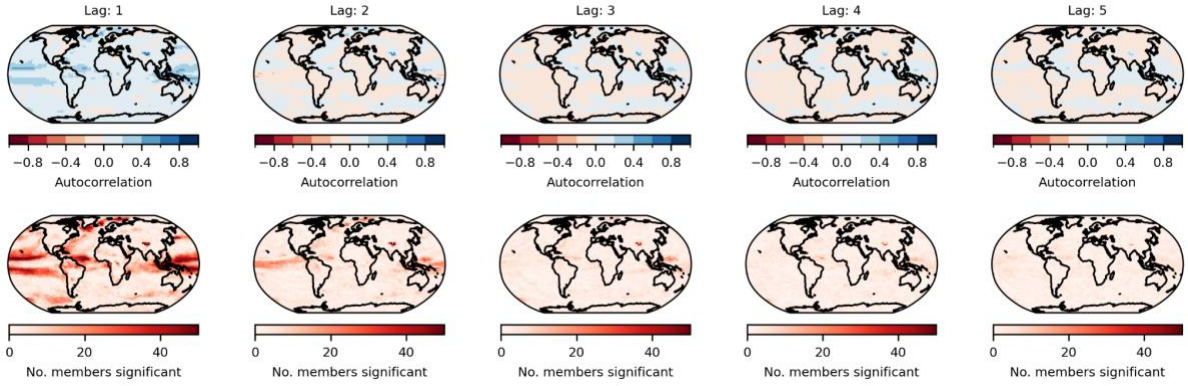

Fig. A4. Autocorrelation of the residuals of the global temperature to local extremes regression for the CanESM5 model. Details as in Fig. A2.

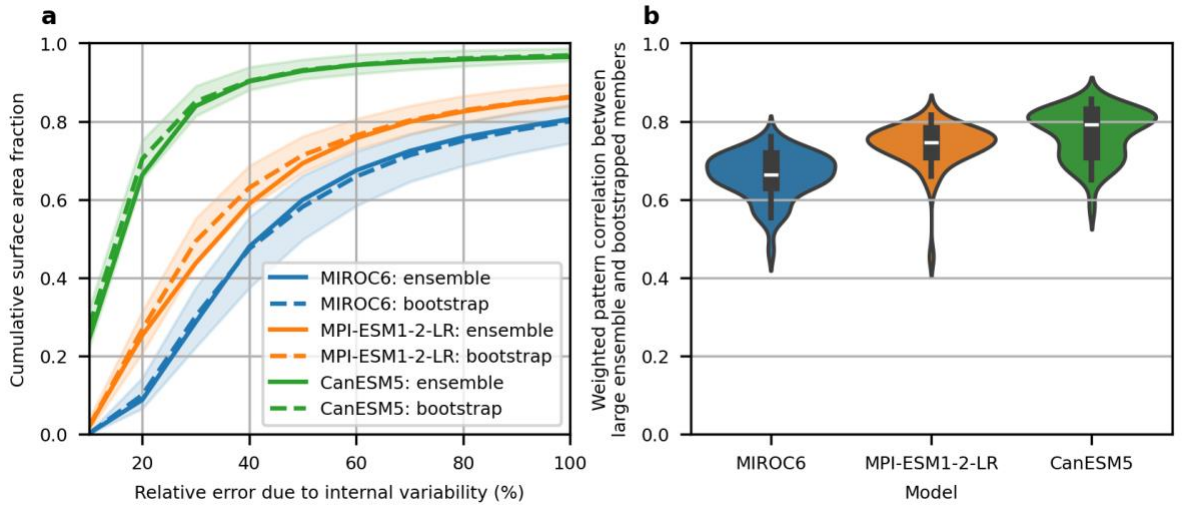

Figure A5. Uncertainty in temperature extreme frequency attribution when using a block-bootstrap with block width of 1 year. Figure is otherwise as Figure 3.

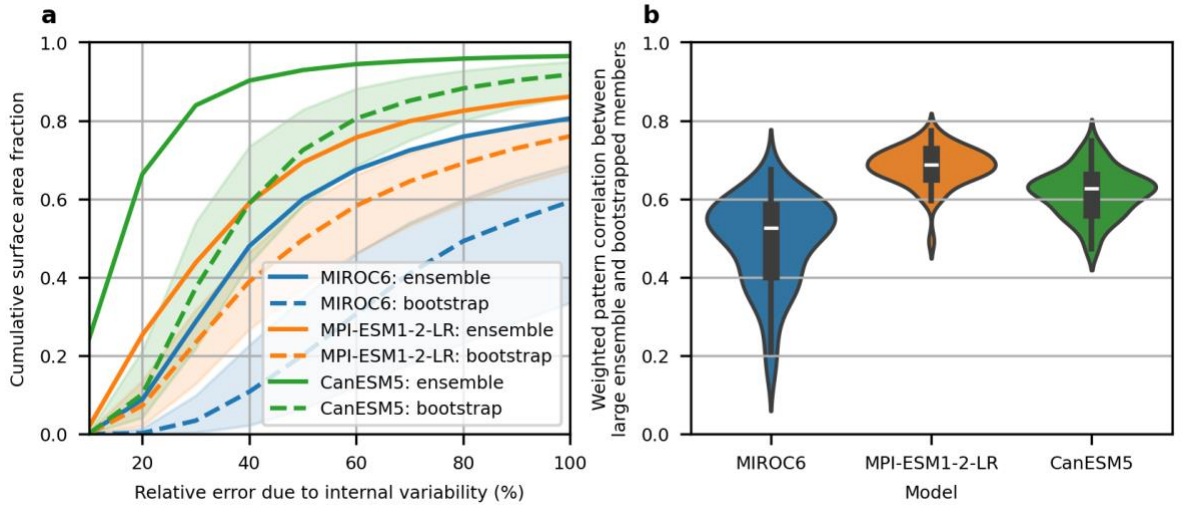

Figure A6. Uncertainty in temperature extreme frequency attribution when using a block-bootstrap with block width of 10 years. Figure is otherwise as Figure 3.

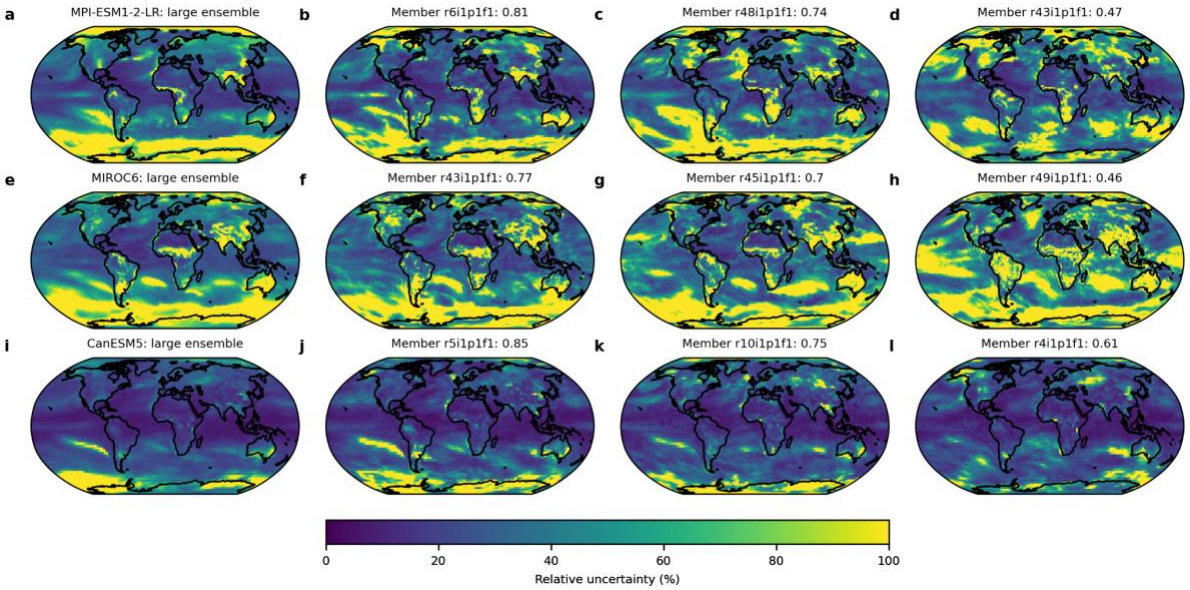

Figure A7. Relative uncertainty in temperature extreme intensity attribution due to internal variability; as reflected in large ensembles and block-bootstrapping of individual ensemble members. As Figure 2 of the main manuscript but for the intensity metric $TX5d$. Results are shown for a block width of 5, based on an assessment of the autocorrelation of residuals as outlined in the manuscript.

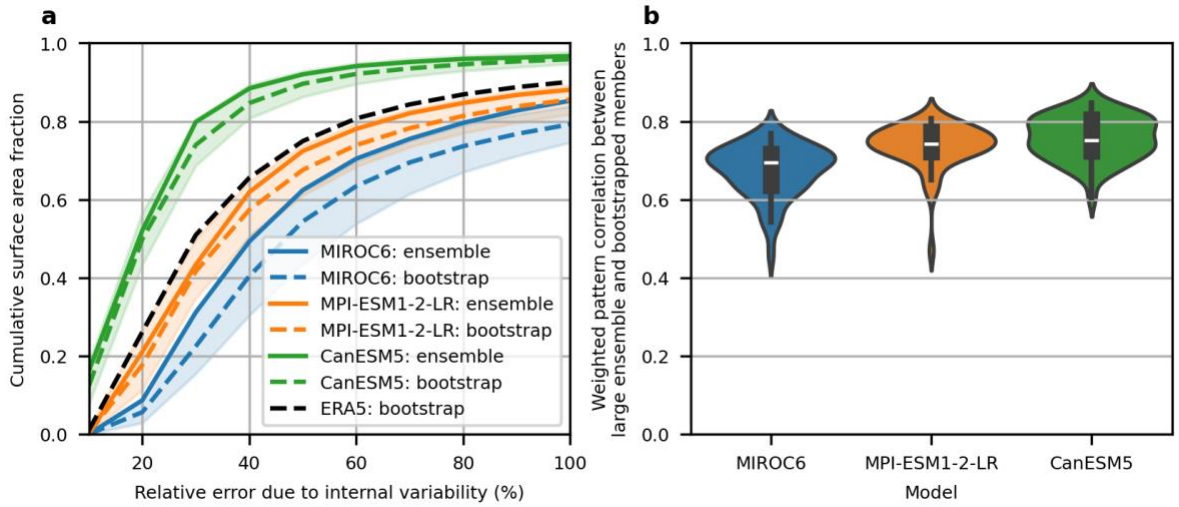

Figure A8. Comparing uncertainty in temperature extreme intensity attribution between the large ensemble and the block-bootstrapping of individual ensemble members. As Figure 3 of the main manuscript but for the temperature extreme intensity metric $TX5d$.

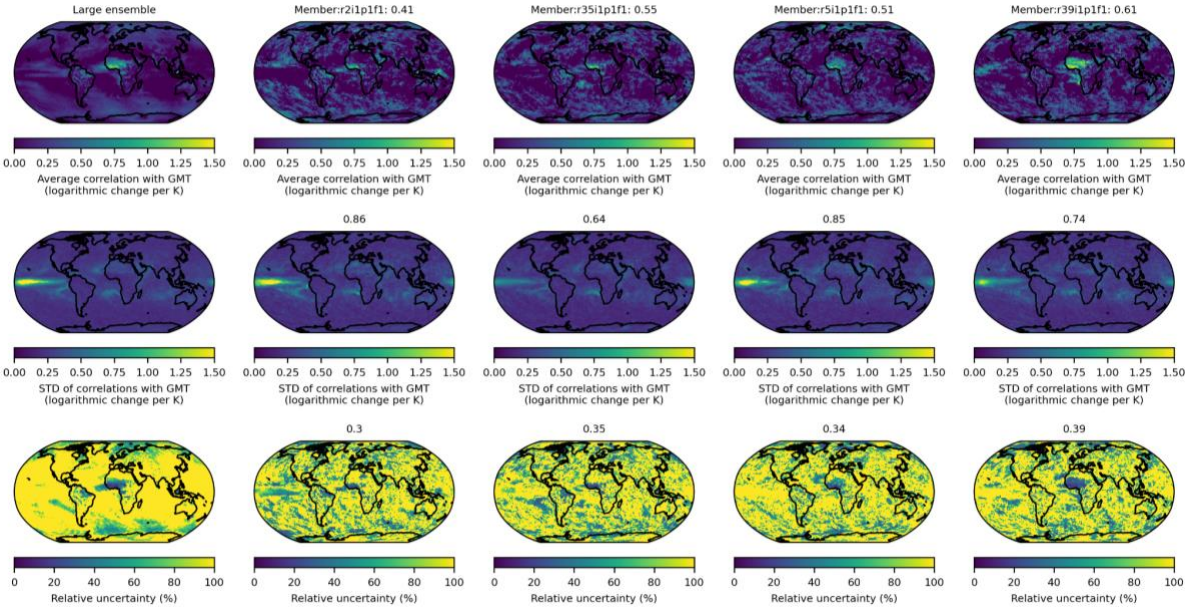

Figure A9. Composition of relative uncertainty for precipitation extreme frequency in the large ensemble and block-bootstrap approaches. Average (upper row), standard deviation (second row), and relative uncertainties (lower row) of correlations between global temperatures and precipitation extremes. Estimates from the true large ensemble (left column) and for four examples of individual ensemble members to which the block-bootstrap procedure has been applied.

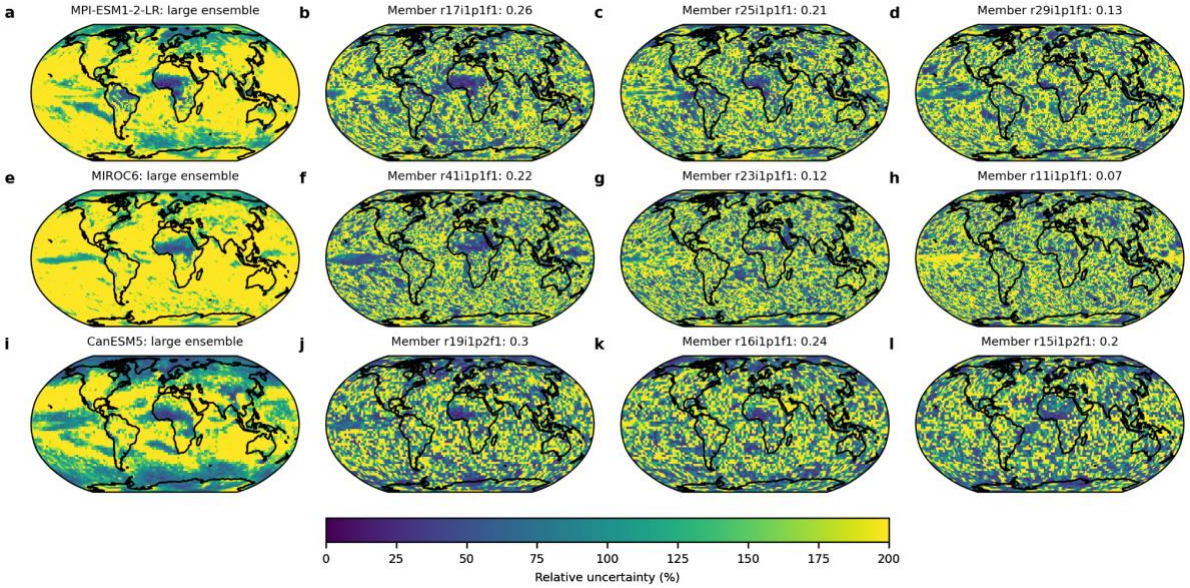

Figure A10. Relative uncertainty in precipitation extreme intensity attribution due to internal variability; as reflected in large ensembles and block-bootstrapping of individual ensemble members. As Figure 4 of the main manuscript but for the intensity metric $PX5d$. Results are shown for a block width of 2, based on an assessment of the autocorrelation of residuals as outlined in the manuscript.

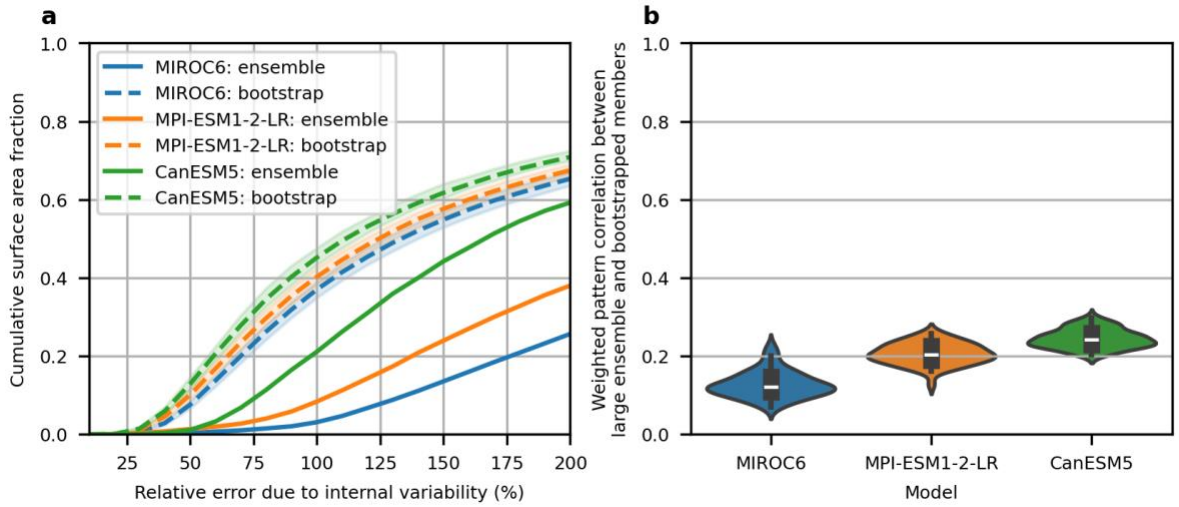

Figure A11. Comparing uncertainty in precipitation extreme intensity attribution between the large ensemble and the block-bootstrapping of individual ensemble members. As Figure 5 of the main manuscript but for the temperature extreme intensity metric $PX5d$.

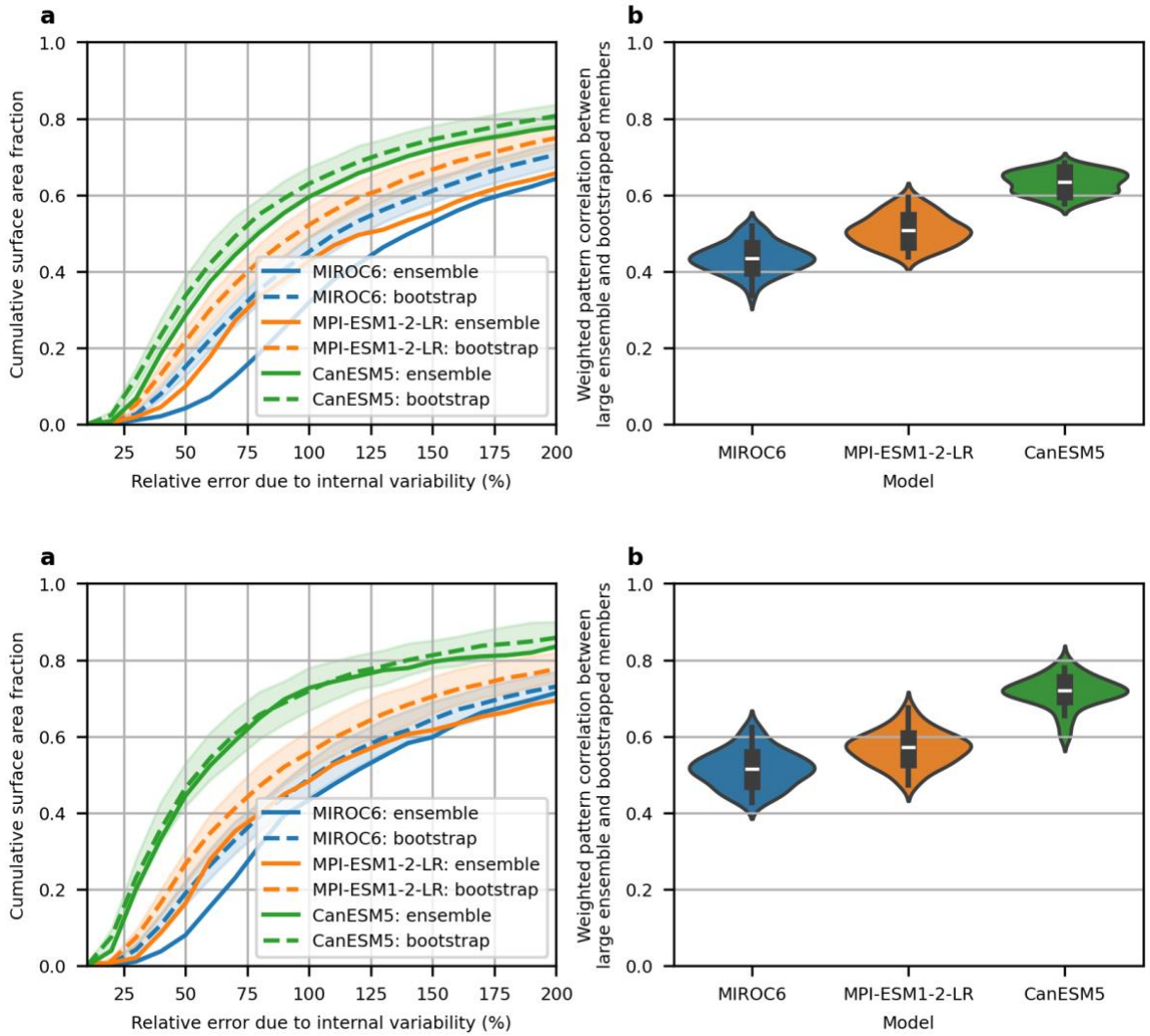

Figure A12. Comparing uncertainty in precipitation extreme frequency attribution when using spatial aggregation. As Figure 5 of the main manuscript but having first aggregated precipitation extreme frequency ($P99p$) to approximately five (upper) and ten (lower) degree grid-cells. We average climate extremes over N adjacent grid-cells where $N \approx \frac{5}{r}, \frac{10}{r}$ (with r the native model resolution) before applying the attribution and other analytical procedures.

REFERENCES

Bartlett, M. S., 1946: On the theoretical specification and sampling properties of autocorrelated time-series. *Suppl. J. R. Stat. Soc.*, **8**, 27–41.

Beck, T. M., D. L. Schumacher, H. Achebak, A. M. Vicedo–Cabrera, S. I. Seneviratne, and J. Ballester, 2024: Mortality burden attributed to anthropogenic warming during Europe's 2022 record-breaking summer. *NPJ Clim. Atmospheric Sci.*, **7**, 245.

Beyer, R., M. T. Miranda Espinosa, S. Ponserre, M. Mengel, and A. Milan, 2024: Heterogeneous effects of climate change on displacement-inducing disasters. *Front. Clim.*, **6**, 1260028.

Byers, E., M. Werning, M. Perrette, N. Schwind, V. Krey, K. Riahi, and C.-F. Schleussner, 2025: Fast climate impact emulation for global temperature scenarios with the rapid impact model emulator (RIME). *Environ. Res. Clim.*, **4**, 035011.

Callahan, C. W., and J. S. Mankin, 2022a: Globally unequal effect of extreme heat on economic growth. *Sci. Adv.*, **8**, eadd3726.

Callahan, C. W., and J.S. Mankin 2022b: National attribution of historical climate damages. *Clim. Change*, **172**, 1–19.

Callahan, C. W., and J.S. Mankin, 2025: Carbon majors and the scientific case for climate liability. *Nature*, **640**, 893–901.

Carlson, C. J., and Coauthors, 2025: Health losses attributed to anthropogenic climate change. *Nat. Clim. Change*, 1–4.

Clarke, B., F. Otto, R. Stuart-Smith, and L. Harrington, 2022: Extreme weather impacts of climate change: an attribution perspective. *Environ. Res. Clim.*, **1**, 012001.

Copernicus, 2025: Copernicus: 2024 is the first year to exceed 1.5°C above pre-industrial level.

Dasgupta, S., N. van Maanen, S. N. Gosling, F. Piontek, C. Otto, and C.-F. Schleussner, 2021: Effects of climate change on combined labour productivity and supply: an empirical, multi-model study. *Lancet Planet. Health*, **5**, e455–e465.

562 Davenport, F. V., M. Burke, and N. S. Diffenbaugh, 2021: Contribution of historical
563 precipitation change to US flood damages. *Proc. Natl. Acad. Sci.*, **118**, e2017524118.

564 Deser, C., A. Phillips, V. Bourdette, and H. Teng, 2012: Uncertainty in climate change
565 projections: the role of internal variability. *Clim. Dyn.*, **38**, 527–546.

566 Deser, C., and Coauthors, 2020: Insights from Earth system model initial-condition large
567 ensembles and future prospects. *Nat. Clim. Change*, **10**, 277–286.

568 Diffenbaugh, N. S., and M. Burke, 2019: Global warming has increased global economic
569 inequality. *Proc. Natl. Acad. Sci.*, **116**, 9808–9813.

570 Dimitrova, A., A. Dimitrova, M. Mengel, A. Gasparrini, H. Lotze-Campen, and S. Gabrysch,
571 2024: Temperature-related neonatal deaths attributable to climate change in 29 low-
572 and middle-income countries. *Nat. Commun.*, **15**, 5504.

573 Donat, M. G., C. Delgado-Torres, P. De Luca, R. Mahmood, P. Ortega, and F. J. Doblas-
574 Reyes, 2023: How credibly do CMIP6 simulations capture historical mean and
575 extreme precipitation changes? *Geophys. Res. Lett.*, **50**, e2022GL102466.

576 Eyring, V., S. Bony, G. A. Meehl, C. A. Senior, B. Stevens, R. J. Stouffer, and K. E. Taylor,
577 2016: Overview of the Coupled Model Intercomparison Project Phase 6 (CMIP6)
578 experimental design and organization. *Geosci. Model Dev.*, **9**, 1937–1958.

579 Fischer, E. M., U. Beyerle, and R. Knutti, 2013: Robust spatially aggregated projections of
580 climate extremes. *Nat. Clim. Change*, **3**, 1033–1038.

581 Gillett, N. P., and Coauthors, 2016: The detection and attribution model intercomparison
582 project (DAMIP v1. 0) contribution to CMIP6. *Geosci. Model Dev.*, **9**, 3685–3697.

583 Hawkins, E., and R. Sutton, 2009: The potential to narrow uncertainty in regional climate
584 predictions. *Bull. Am. Meteorol. Soc.*, **90**, 1095–1108.

585 Hersbach, H., and Coauthors, 2020: The ERA5 global reanalysis. *Q. J. R. Meteorol. Soc.*,
586 **146**, 1999–2049.

587 King, A. D., M. R. Grose, J. Kimutai, I. Pinto, and L. J. Harrington, 2023: Event attribution is
588 not ready for a major role in loss and damage. *Nat. Clim. Change*, **13**, 415–417.

589 Kotz, M., L. Wenz, and A. Levermann, 2021: Footprint of greenhouse forcing in daily
590 temperature variability. *Proc. Natl. Acad. Sci.*, **118**, e2103294118.

591 Kotz, M, A. Levermann, and L. Wenz, 2022: The effect of rainfall changes on economic
592 production. *Nature*, **601**, 223–227.

593 Kotz, M, T. Amano, and J. E. Watson, 2025: Large reductions in tropical bird abundance
594 attributable to heat extreme intensification. *Nat. Ecol. Evol.*, 1–13.

595 Lee, H., and Coauthors, 2023: IPCC, 2023: Climate change 2023: Synthesis report, summary
596 for policymakers. Contribution of working groups i, II and III to the sixth assessment
597 report of the intergovernmental panel on climate change [core writing team, h. Lee
598 and j. Romero (eds.)]. IPCC, geneva, Switzerland.

599 Lehner, F., C. Deser, N. Maher, J. Marotzke, E. M. Fischer, L. Brunner, R. Knutti, and E.
600 Hawkins, 2020: Partitioning climate projection uncertainty with multiple large
601 ensembles and CMIP5/6. *Earth Syst. Dyn.*, **11**, 491–508.

602 McKinnon, K. A., and C. Deser, 2018: Internal variability and regional climate trends in an
603 observational large ensemble. *J. Clim.*, **31**, 6783–6802.

604 McKinnon, K. A., A. Poppick, E. Dunn-Sigouin, and C. Deser, 2017: An "observational large
605 ensemble" to compare observed and modeled temperature trend uncertainty due to
606 internal variability. *J. Clim.*, **30**, 7585–7598.

607 Mengel, M., S. Treu, S. Lange, and K. Frieler, 2021: ATTRICI v1. 1–counterfactual climate
608 for impact attribution. *Geosci. Model Dev.*, **14**, 5269–5284.

609 Murali, G., T. Iwamura, S. Meiri, and U. Roll, 2023: Future temperature extremes threaten
610 land vertebrates. *Nature*, **615**, 461–467.

611 Noy, I., M. Wehner, D. Stone, S. Rosier, D. Frame, K. A. Lawal, and R. Newman, 2023:
612 Event attribution is ready to inform loss and damage negotiations. *Nat. Clim. Change*,
613 **13**, 1279–1281.

614 Ortiz-Bobea, A., T. R. Ault, C. M. Carrillo, R. G. Chambers, and D. B. Lobell, 2021:
615 Anthropogenic climate change has slowed global agricultural productivity growth.
616 *Nat. Clim. Change*, **11**, 306–312.

617 Park, C. Y., and Coauthors, 2024: Attributing human mortality from fire PM2. 5 to climate
618 change. *Nat. Clim. Change*, **14**, 1193–1200.

619 Quilcaille, Y., and Coauthors, 2025: Systematic attribution of heatwaves to the emissions of
620 carbon majors. *Nature*, **645**, 392–398.

621 Riahi, K., and Coauthors, 2017: The shared socioeconomic pathways and their energy, land
622 use, and greenhouse gas emissions implications: an overview. *Glob. Environ. Change*,
623 **42**, 153–168.

624 Schwalm, C. R., S. Glendon, and P. B. Duffy, 2020: RCP8. 5 tracks cumulative CO2
625 emissions. *Proc. Natl. Acad. Sci.*, **117**, 19656–19657.

626 Seneviratne, S. I., M. G. Donat, A. J. Pitman, R. Knutti, and R. L. Wilby, 2016: Allowable
627 CO2 emissions based on regional and impact-related climate targets. *Nature*, **529**,
628 477–483.

629 Tavoni, M., P. Andreoni, M. Calcaterra, E. Calliari, T. Deubelli-Hwang, R. Mechler, S.
630 Hochrainer-Stigler, and L. Wenz, 2024: Economic quantification of Loss and Damage
631 funding needs. *Nat. Rev. Earth Environ.*, **5**, 411–413.

632 Tebaldi, C., and J. M. Arblaster, 2014: Pattern scaling: Its strengths and limitations, and an
633 update on the latest model simulations. *Clim. Change*, **122**, 459–471.

634 Trok, J. T., E. A. Barnes, F. V. Davenport, and N. S. Diffenbaugh, 2024: Machine learning–
635 based extreme event attribution. *Sci. Adv.*, **10**, eadl3242.

636 Wills, R. C., D. S. Battisti, K. C. Armour, T. Schneider, and C. Deser, 2020: Pattern
637 recognition methods to separate forced responses from internal variability in climate
638 model ensembles and observations. *J. Clim.*, **33**, 8693–8719.

639 Wills, R. C., Y. Dong, C. Proistosecu, K. C. Armour, and D. S. Battisti, 2022: Systematic
640 climate model biases in the large-scale patterns of recent sea-surface temperature and
641 sea-level pressure change. *Geophys. Res. Lett.*, **49**, e2022GL100011.

642 Wills, R. C., and Coauthors, 2025: Forced Component Estimation Statistical Method
643 Intercomparison Project (ForceSMIP). *Authorea Prepr.*